International Journal of Solids and Structures 51 (2014) 3679–3688

Contents lists available at ScienceDirect

International Journal of Solids and Structures

journal homepage: www.elsevier.com/locate/ijsolstr

Multi-level modeling of woven glass/epoxy composite for multilayer printed circuit board applications

Zhuo Chen, Fan Yang, S.A. Meguid *

Mechanics and Aerospace Design Laboratory, Mechanical and Industrial Engineering, University of Toronto, 5 King's College Rd, Toronto, Ontario M5S 3G8, Canada

ARTICLE INFO

Article history:
Received 27 February 2014
Received in revised form 16 June 2014
Available online 9 July 2014

Keywords:
Micromechanics
Homogenization
Finite element method
Woven composite
Multilayer PCB

ABSTRACT

The objective of this paper is to develop a hybrid homogenization method to predict the elastic properties of a common woven glass/epoxy composite substrate for multilayer circuit board applications. Comprehensive high resolution 3D finite element (FE) models of a quarter of the repeated unit cell (RUC) for the woven glass/epoxy composite were developed based on different micromechanical schemes. . Specifically, four different micromechanics schemes were investigated: self-consistent, Mori–Tanaka, three-phase approach and composite cylinder assemblage (CCA). The element based strain concentration matrices were determined and used to obtain the homogenized woven glass/epoxy composite properties via a specially developed MATLAB code. Attention was further devoted to the predictions of the homogenized elastic moduli of the multilayer printed circuit board (PCB). The results from our simulations, based on Mori–Tanaka and CCA, are in good agreement with existing experimental results, indicating that the newly proposed homogenization scheme can be used as a design tool to predict the overall properties of woven composite materials typically used in multilayer PCB applications.

1. Introduction

Multilayer printed circuit board (PCB) has been used extensively in electronic packaging assemblies, and its mechanical reliability has become an important issue in industry (Harris and Pierosol, 2002). The deflection of boards could lead to the failure of the mounted electronics, especially in drop conditions (Blackketter et al., 1993). The microstructure of a multilayer laminate in PCB is a combination of copper foils and composite plies consisting of woven glass/epoxy substrate (Zhu et al., 2003). In most literature, multilayer PCB has been modeled as a simplified single layer board using isotropic (Wang et al., 2003, 2006) or orthotropic material models (Lee, 2000) without considering its complex composite microstructure.

Several analytical models have been developed in the literature to investigate the mechanical properties of woven composite. Ishikawa and Chou (1982a,b, 1983a,b) have proposed two one-dimensional models: the mosaic model and the fiber undulation model. In the mosaic model, the woven fabric is idealized as an assemblage of asymmetrical cross-ply laminates neglecting the continuity and undulation of the fiber bundles. The fiber undulation model accounts for the continuity and undulation of fibers in a fabric, while it was suitable only for weaves with a lower number of repeats. Naik and Shembekar (1992a,b, 1993) improved the fiber undulation model by considering the two-dimensional extent of the fabric. The various parameters of fabric geometry, including gaps between the fiber bundles, laminate configuration were taken into account and their effects were examined. Naik and Shembekar (1992a,b, 1993) further extended the method to predict the thermal expansion coefficients.

Sottos et al. (1999) introduced two micromechanical models for predicting the thermo-elastic properties of woven glass laminates. The "equivalent" laminate model (EQLAM) used the simplified representation of the woven fabric laminate with a symmetric three-ply crossply laminate. The overall properties of the laminate are then obtained using classical lamination theory. The basic strategy of the blending model (BLEND) is to first calculate the intermediate matrix using the properties of the fill bundles. The warp bundles are assumed to reinforce this intermediate fill ply. Then instead of using lamination theory, Halpin–Tsai equations were used to combine the warp fiber properties with the calculated properties for the intermediate fill ply. The Euler–Bernoulli beam theory was employed in the theoretical model proposed by Lee and Harris (1988) to predict the effective moduli of composite laminates with wavy patterns. The principle of minimum potential energy was applied to calculate the displacement field of the curved beam and to obtain the effective moduli of the composite.

* Corresponding author.
E-mail address: meguid@mie.utoronto.ca (S.A. Meguid).

http://dx.doi.org/10.1016/j.ijsolstr.2014.06.030
0020-7683/

Ito and Chou (1997) employed the curved beam model to determine the effective moduli and the stress field for plain-weave composites under tension loading.

Computational studies have also been utilized to determine the mechanical properties of woven composites. For example, Shindo et al. (1993) investigated the thermo-mechanical response of non-metallic woven composites with temperature-dependent properties using finite element method. Sankar and Marrey (1993) used a two-dimensional FE model of a unit cell to determine the flexural stiffness coefficients of the composite beam. Dasgupta et al. (1996) determined the effective thermo-mechanical properties of plain-weave fabric-reinforced composite laminates obtained based on micromechanical analyses. The effective orthotropic tensors for stiffness, coefficient of thermal expansion and thermal conductivity were all obtained using appropriate averaging schemes. Low and Wang (2008) presented a hybrid modeling method to describe the behavior of multilayer multi-material composites containing both metallic and woven composite plies.

Existing analytical models (see, e.g., Sottos et al., 1999; Ishikawa and Chou, 1982; Naik and Shembekar, 1992a,b) are grossly oversimplified such as by degenerating the system into a 2D problem and neglecting the continuity and undulation of the fiber bundles. The numerical model developed in Low and Wang (2008) is also based on some of the simplified analytical results in Sottos et al. (1999), and it can be only used to predict the in-plane material properties. In contrast, our work is more rigorous. For example, the homogenization is carried out in three levels thus emphasizing the complex nature of the PCB structure. The PCB is actually a multi-level composite material. It is composed of multi-layers with each layer composed of the matrix and the woven fiber bundles. The fiber bundle is also a composite material if viewed at the smaller scale dimension. It is composed of the fiber phase (fibers) and the epoxy phase. In order to obtain the effective properties of the fiber bundles, a number of analytical/semi-analytical micromechanical schemes were developed. Among these efforts, several micromechanics schemes were widely used, e.g., the self-consistent scheme (Hill, 1965), the Mori–Tanaka scheme (Mori and Tanaka, 1973), the three phase scheme (Christensen and Lo, 1979), and the composite cylinder assemblage scheme (CCA scheme) (Hashin, 1965).

In this paper, we developed a bottom-up multi-level micromechanics based homogenization model to determine the equivalent material property of the multilayer circuit board. Firstly, the effective properties of the fiber bundle were determined using different micromechanical schemes. Secondly, the homogenized elastic properties of woven composite substrate were obtained by solving a FE-based boundary value problem of a unit cell. Finally, the classical laminate theory was accounted for by calculating the multilayer PCB moduli. The results from the different micromechanics schemes were compared with existing experimental data in literature to evaluate the applicability of the different approaches.

This paper is organized as follows. Following this brief introduction, Section 2 developed a combined micromechanical and finite element method to predict the equivalent property of woven composite substrate. Section 3 extends the laminate theory to predict the elastic properties for the multilayer PCB. In Section 4, we conclude the paper.

2. Homogenization of woven composite substrate

2.1. Modeling approach

Fig. 1 shows the micromechanical homogenization process employed in this section. Firstly, statistically homogeneous micromechanical schemes were used for the homogenization of fiber bundle scale considering the fiber waviness effect. Secondly, a periodic cell FE model was developed. Due to the complexity of the microstructure, each element is regarded as one phase, and strain concentration matrices based on each finite element is computed. In order to determine the composite constitutive parameters, we make use of the following expression,

$$C^* = \sum_{i=1}^{n} c_i C^i \bar{A}^i \tag{1}$$

where, C^* is the equivalent composite stiffness matrix, C^i is the stiffness matrix of each phase, c_i is the phase volume fraction, n is the total phase number. $\bar{A}^i$ is the strain concentration matrix of each phase, which is defined as follows:

$$\bar{\varepsilon}^i = \bar{A}^i \bar{\varepsilon} \tag{2}$$

$$\text{i.e.,} \quad \begin{bmatrix} \bar{\varepsilon}_1^i \\ \bar{\varepsilon}_2^i \\ \bar{\varepsilon}_3^i \\ \bar{\varepsilon}_4^i \\ \bar{\varepsilon}_5^i \\ \bar{\varepsilon}_6^i \end{bmatrix} = \begin{bmatrix} A_{11} & A_{12} & A_{13} & A_{14} & A_{15} & A_{16} \\ A_{21} & A_{22} & A_{23} & A_{24} & A_{25} & A_{26} \\ A_{31} & A_{32} & A_{33} & A_{34} & A_{35} & A_{36} \\ A_{41} & A_{42} & A_{43} & A_{44} & A_{45} & A_{46} \\ A_{51} & A_{52} & A_{53} & A_{54} & A_{55} & A_{56} \\ A_{61} & A_{62} & A_{63} & A_{64} & A_{65} & A_{66} \end{bmatrix} \begin{bmatrix} \bar{\varepsilon}_1 \\ \bar{\varepsilon}_2 \\ \bar{\varepsilon}_3 \\ \bar{\varepsilon}_4 \\ \bar{\varepsilon}_5 \\ \bar{\varepsilon}_6 \end{bmatrix}$$

where, $\bar{\varepsilon}^i$ is the strain of each phase and $\bar{\varepsilon}$ is the averaged strain applied on the boundary.

2.2. Micromechanical modeling of fiber bundles

2.2.1. Unidirectional fiber bundle homogenization

The composite substrates used in circuit board applications are composed of epoxy matrix reinforced with plain-weave glass fabrics. The fill and warp fiber bundles interlace with each other in an orthogonal way. The microstructure of the substrate containing both fiber phase and matrix phase is illustrated in Fig. 2. It is computational prohibitive to explicitly consider the large number of fibers in the fiber phase in the model. Therefore, our model is first developed based on the homogenization of the fiber bundles. In this study, the properties of one common fabric style 7628, were investigated. Table 1 shows the geometric dimensions and volume fractions of the fiber phase used in the model (Shrotriya, 2001).

In order to obtain the equivalent properties of fiber bundles, different micromechanical schemes were used and compared i.e., the self-consistent scheme, the Mori–Tanaka scheme, the three phase scheme, and the composite cylinder assemblage scheme (CCA scheme). The Hashin–Shtrikman bounds were also calculated to examine each micromechanical scheme. Since the abovementioned schemes are only valid for unidirectional fiber reinforced composite without considering the waviness of the geometry, it is worth mentioning that the fiber bundles in this section were considered as transverse isotropic material. The waviness effect is considered in the next section. Table 2 provides the effective isotropic constitutive parameters for both the fiber phase and the epoxy matrix phase.

As shown in Fig. 3, it could be observed that all the schemes yield results within the range of Hashin–Shtrikman bounds. Under transverse loading, only upper and lower bounds may be obtained using CCA scheme because the single composite cylinder ceases to respond like an RVE under homogeneous displacement or homogeneous traction boundary conditions. Therefore, the three phase model in this case is used to predict the transverse shear moduli, and combined with CCA scheme to provide all the homogenized constitutive parameters. It is found that the Mori–Tanaka and CCA/three phase schemes yield similar results for homogenized properties, while there is a larger discrepancy for the self-consistent scheme result, especially at high inclusion concentrations. In our model, the fiber volume fraction is 75%.

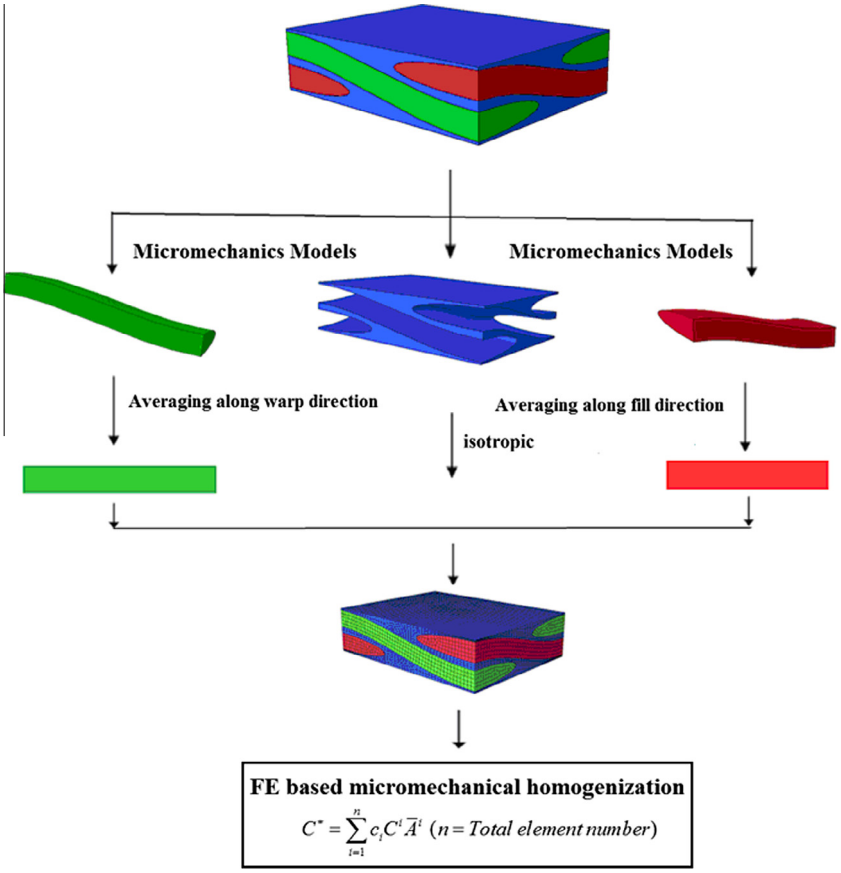

Fig. 1. Demonstration of joint micromechanical FE modeling approach.

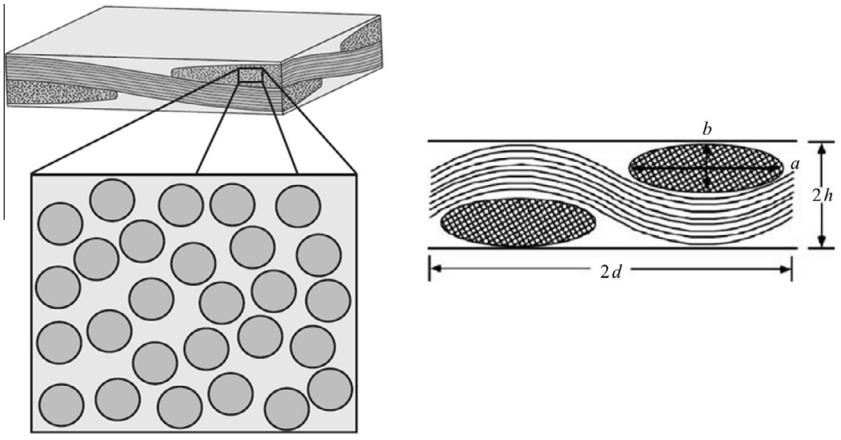

Fig. 2. Schematic of plain-weave geometry (Shindo et al., 1993).

2.2.2. Waviness effect

The waviness of warp and fill would play an important role in determining the overall property. Therefore, it is the objective of this section to account for the effect of fiber waviness. Fig. 4 shows a schematic of an undulating fiber bundle (x–z plane). The curve of undulation can be described by,

$$z(x) = \frac{h}{2}\cos\left(\frac{\pi}{d}x\right) \tag{3}$$

where h and d are the thickness and the length of a unit composite cell, respectively. Assuming the fibers are straight and oriented at angle θ over a small section dx of the bundle, the angle can be described by the slope of the curve; viz.,

$$\theta(x) = -\tan^{-1}\left(\frac{dz}{dx}\right) \tag{4}$$

Table 1
Bundle sizes, crimp geometry, and fiber volume fractions.

	Aspect ratio a/b	Crimp h/d	Fiber volume fraction in composite	Fiber volume fraction in bundle
Warp	5.26	0.053	0.754	0.268
Fill	7.26	0.083	0.759	0.194

Table 2
Elastic properties of glass fibers and epoxy matrix (Dasgupta et al., 1996).

Constituent	E (GPa)	v
Fiber	72.3	0.22
Matrix	3.05	0.33

An orientation averaging scheme was employed. Firstly, coordinate transformations were used to determine the properties of the small segment after rotation at position x along the length of the ply. According to tensor theory, the fourth-order stiffness tensor obeys the following transformation scheme:

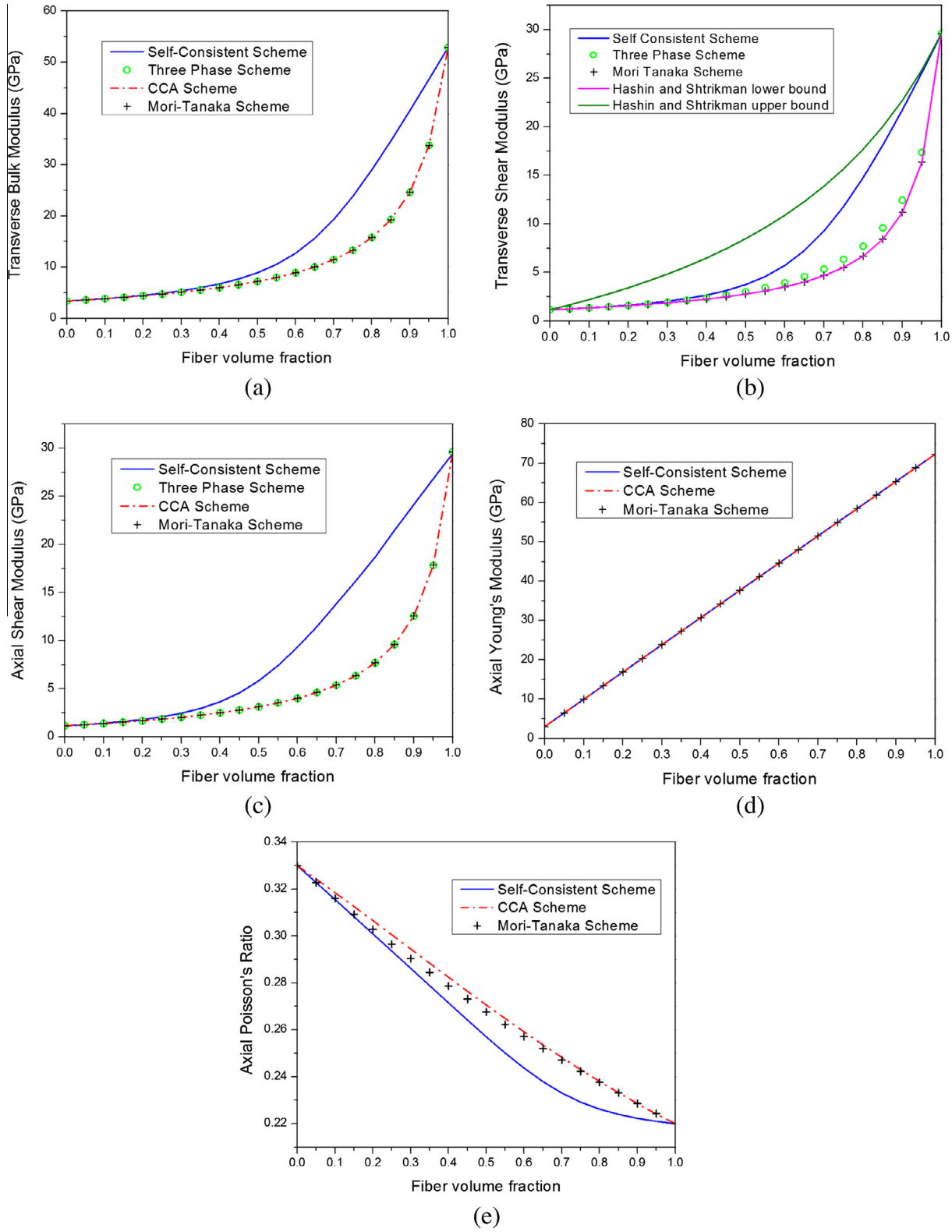

Fig. 3. Homogenized properties of fiber bundles using different micromechanical schemes for: (a) transverse bulk modulus, (b) transverse shear modulus, (c) axial shear modulus, (d) axial Young's modulus, and (e) axial Poisson's ratio.

$$c'_{ijkl} = c_{mnsp} l_{im} l_{jn} l_{ks} l_{lp} \tag{5}$$

Reducing the indices of stiffness tensor, the above transformation equation can be rewritten as (Cowin, 2013):

$$c'_{ij} = c_{mn} t^{c}_{im} t^{c}_{jn} \tag{6}$$

where $l_{ij} = \cos(x'_i, x_j)$,

$$t^{c}_{ij} = \begin{bmatrix} l_{11}^2 & l_{12}^2 & l_{13}^2 & 2l_{12}l_{13} & 2l_{13}l_{11} & 2l_{12}l_{11} \\ l_{21}^2 & l_{22}^2 & l_{23}^2 & 2l_{23}l_{22} & 2l_{23}l_{21} & 2l_{22}l_{21} \\ l_{31}^2 & l_{32}^2 & l_{33}^2 & 2l_{33}l_{32} & 2l_{33}l_{31} & 2l_{32}l_{31} \\ l_{31}l_{21} & l_{32}l_{22} & l_{33}l_{23} & l_{33}l_{22}+l_{32}l_{23} & l_{33}l_{21}+l_{31}l_{23} & l_{31}l_{22}+l_{32}l_{21} \\ l_{31}l_{11} & l_{32}l_{12} & l_{33}l_{13} & l_{33}l_{12}+l_{32}l_{13} & l_{33}l_{11}+l_{31}l_{13} & l_{31}l_{12}+l_{32}l_{11} \\ l_{21}l_{11} & l_{12}l_{22} & l_{13}l_{23} & l_{13}l_{22}+l_{12}l_{23} & l_{13}l_{21}+l_{11}l_{23} & l_{11}l_{22}+l_{12}l_{21} \end{bmatrix}$$

Secondly, the effective stiffness matrix of the warp and fill bundles are computed by averaging the rotated properties along the length direction as follows:

$$\bar{C}^{k}_{ij} = \frac{1}{2d}\int_0^{2d} C'^{k}_{ij}(x)\mathrm{d}x \tag{7}$$

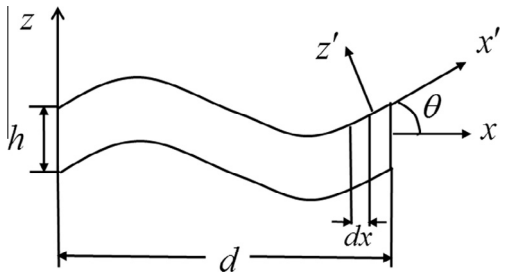

Fig. 4. A schematic of the undulating bundle.

Table 3
Orientation averaged Young's moduli of the warp and fill fiber bundles.

Micromechanical schemes	Fiber bundle	E_x (GPa)	E_y (GPa)	E_z (GPa)
Self-consistent scheme	Warp	54.30	30.96	30.67
	Fill	30.67	31.15	53.70
Mori Tanaka scheme	Warp	52.91	15.27	15.38
	Fill	15.43	15.24	51.55
CCA/three phase scheme	Warp	52.91	16.75	16.92
	Fill	16.95	16.69	51.54

where, $C'^{k}_{ij}(x)$ is the stiffness matrix of the fiber bundle along the fiber direction. $\bar{C}^{k}_{ij}$ is the averaged stiffness matrix of the wavy fiber bundle. Table 3 shows orientation averaged Young's moduli of the warp and fill, which were the input material properties in our FE model.

2.3. Finite element modeling

2.3.1. Periodic cell model

Micromechanical analyses of periodic heterogeneous materials were mainly conducted based on the concept of repeated unit cell

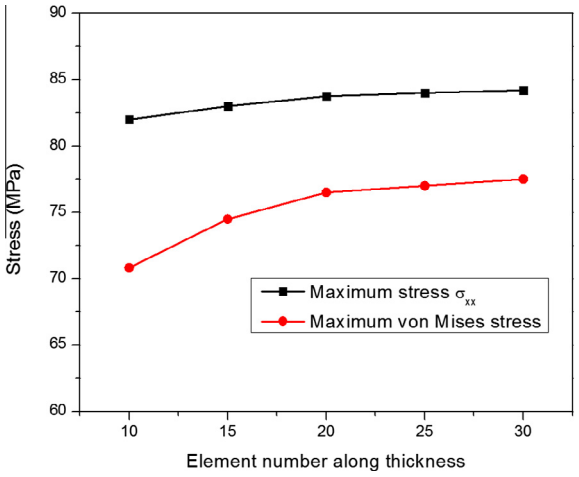

Fig. 6. Element size convergence study of unit cell model.

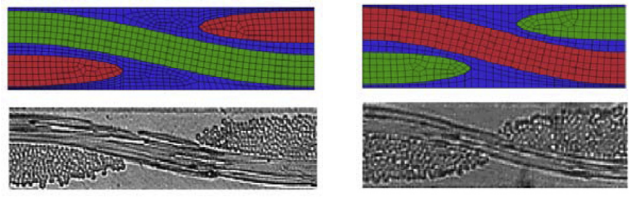

(a) Warp parallel face (b) Fill parallel face

Fig. 7. Comparison between FE model and experimental sample for: (a) warp parallel face, and (b) fill parallel face.

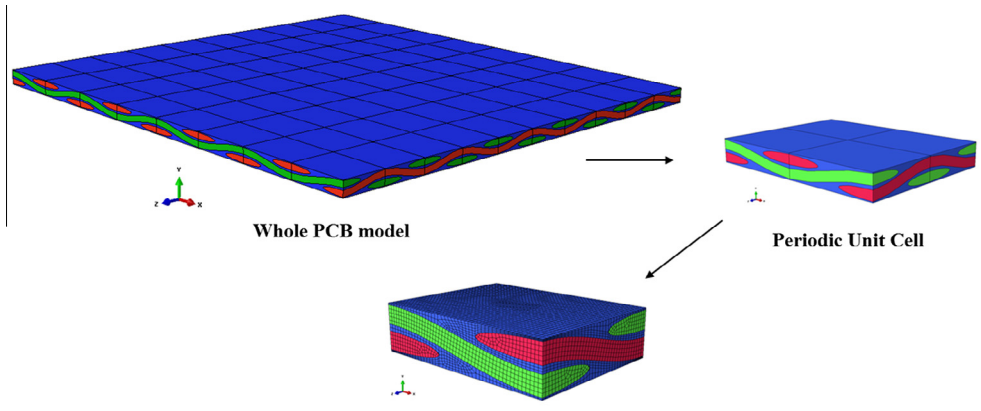

Fig. 5. FE model of periodic cell model.

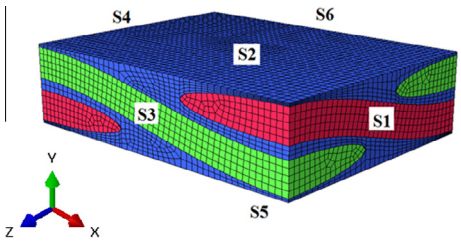

Fig. 8. Lateral boundaries in FE model.

(RUC). In our case, the woven composite substrate was modeled using a unit cell with periodic boundary conditions. Furthermore, due to symmetry of the microstructure, one quarter of the RUC (see Fig. 5) is sufficient for our analyses using symmetric boundary conditions.

The model is discretized using eight-noded solid elements with reduced integration scheme (element type C3D8R). The reduced integration scheme dramatically reduced the computation cost without showing discernible differences in the results obtained using full-integration scheme. The length of the quarter periodic cell was selected to be 1.69 mm along the warp direction and 1.08 mm along the fill direction. The thickness of the cell model was taken to be 0.18 mm. In order to obtain accurate and compatible displacement and stress fields in each unit cell, a sufficiently refined FE mesh was employed to discretize the multi-phased cell. In Fig. 6, we conducted the convergence study and examined the stress values (von Mises stress or stress σ_{xx}) by stretching the unit cell with a predetermined displacement of 0.018 mm along the x-direction. The mesh was subsequently refined until the percentage variation in the stress values is less than 1%. The final meshing density of our model was selected using 20 elements along the thickness with a minimum element size of about 0.01 mm. The displacement continuity and traction continuity are guaranteed on the fiber/matrix interface by mesh consistency. A comparison between the microstructure of our FE model and that of the experimental sample of Sottos et al. (1999) is shown in Fig. 7.

2.3.2. Boundary conditions

The analysis was performed on a parallel-piped of fixed dimensions (X,Y,Z) with the lateral boundary S (see Fig. 8) given by:

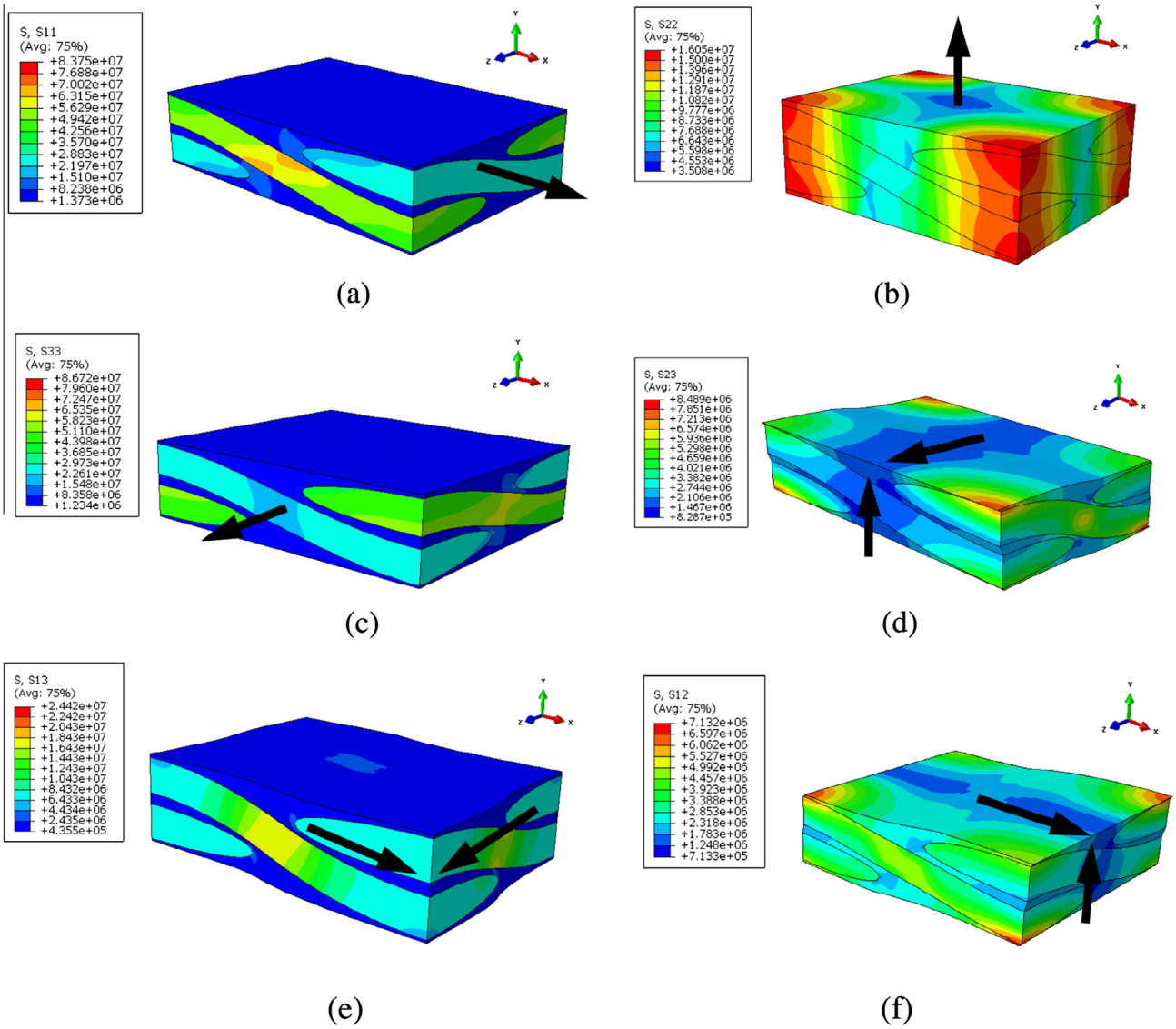

Fig. 9. Stress (Unit: Pa) profiles for the six independent loading conditions (a) $\varepsilon_1 = 0.1$, (b) $\varepsilon_2 = 0.1$, (c) $\varepsilon_3 = 0.1$, (d) $\varepsilon_4 = 0.1$, (e) $\varepsilon_5 = 0.1$, and (f) $\varepsilon_6 = 0.1$, noting that all other strains equal to zero.

Table 4
Homogenized material properties for one composite ply.

	E_{warp} (GPa)	E_{fill} (GPa)	E_{thick} (GPa)
Self-consistent scheme	22.2	21.0	8.55
Mori–Tanaka scheme	18.6	16.9	7.05
CCA/three phase scheme	19.2	17.5	7.29

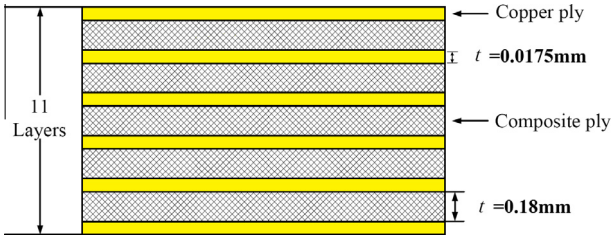

Fig. 10. Schematic of multilayer model (Low and Wang, 2008).

S_1: $0 \leqslant y_1 \leqslant Y$, $0 \leqslant z_1 \leqslant Z$, $x_1 = X$, $n = (0,0,1)$.
S_2: $0 \leqslant x_2 \leqslant X$, $0 \leqslant z_2 \leqslant Z$, $y_2 = Y$, $n = (0,1,0)$.
S_3: $0 \leqslant x_3 \leqslant X$, $0 \leqslant y_3 \leqslant Y$, $z_3 = Z$, $n = (0,0,1)$.
S_4: $0 \leqslant y_1 \leqslant Y$, $0 \leqslant z_1 \leqslant Z$, $x_1 = 0$, $n = (0,0,-1)$.
S_5: $0 \leqslant x_2 \leqslant X$, $0 \leqslant z_2 \leqslant Z$, $y_2 = 0$, $n = (0,-1,0)$.
S_6: $0 \leqslant x_3 \leqslant X$, $0 \leqslant y_3 \leqslant Y$, $z_3 = 0$, $n = (0,0,-1)$.

The symmetric, anti-symmetric and periodic boundary conditions are given explicitly in Appendix B for the six independent loading types. The stress contours for each loading condition are shown in Fig. 9.

3. Results and discussions

Due to the large number of element, a MATLAB code was written to obtain the homogenized stiffness and compliance matrix of the woven composite. In our case, each element in the unit cell was considered as an individual phase. Given the specified six types of loading and boundary conditions, the resulting strain tensor of each element $\bar{\varepsilon}^i$ was obtained and the strain concentration matrices $\bar{A}^i$ for each element were determined using Eq. (2). The homogenized stiffness matrix for the PCB composite substrate was calculated by considering all the element contributions using Eq. (1). As an example, the stiffness and compliance matrix based on CCA scheme are shown below. It can be seen from the matrices that the off-diagonal components corresponding to normal-shear coupling effect are close to zero (small values due to finite element numerical errors).

$$C^{eff} = \begin{bmatrix} 26.2379 & 4.9442 & 6.1132 & 0.0023 & 0.0021 & 0.0000 \\ 4.9442 & 8.5383 & 5.4256 & 0.0010 & 0.0005 & -0.0001 \\ 6.1132 & 5.4256 & 22.7417 & 0.0011 & 0.0008 & -0.0003 \\ 0.0023 & 0.0010 & 0.0011 & 2.2444 & 0.0110 & -0.0020 \\ 0.0021 & 0.0005 & 0.0008 & 0.0110 & 3.4615 & -0.0060 \\ 0.0000 & -0.0001 & -0.0003 & -0.0020 & -0.0060 & 2.2377 \end{bmatrix} \text{GPa},$$

$$S^{eff} = \begin{bmatrix} 0.0436 & -0.0210 & -0.0067 & -0.0000 & -0.0000 & -0.0000 \\ -0.0210 & 0.1482 & -0.0297 & -0.0000 & -0.0000 & 0.0000 \\ -0.0067 & -0.0297 & 0.0529 & -0.0000 & -0.0000 & 0.0000 \\ -0.0000 & -0.0000 & -0.0000 & 0.4456 & -0.0014 & 0.0004 \\ -0.0000 & -0.0000 & -0.0000 & -0.0014 & 0.2889 & 0.0008 \\ -0.0000 & 0.0000 & 0.0000 & 0.0004 & 0.0008 & 0.4469 \end{bmatrix} (\text{GPa})^{-1}$$

The orthotropic constitutive law is given in Eq. (8). With the parameter values of the effective compliance matrix given above, nine independent constitutive constants are obtained. Table 4 shows the homogenized parameters from different micromechanics schemes. It can be seen that the self-consistent scheme provides results that are larger than the Mori–Tanaka and CCA schemes. Since self-consistent scheme essentially assumes that a single inclusion is embedded in an infinite equivalent homogenized medium. Therefore, it does not account for the inclusion interaction. The discrepancy could be attributed to the inability

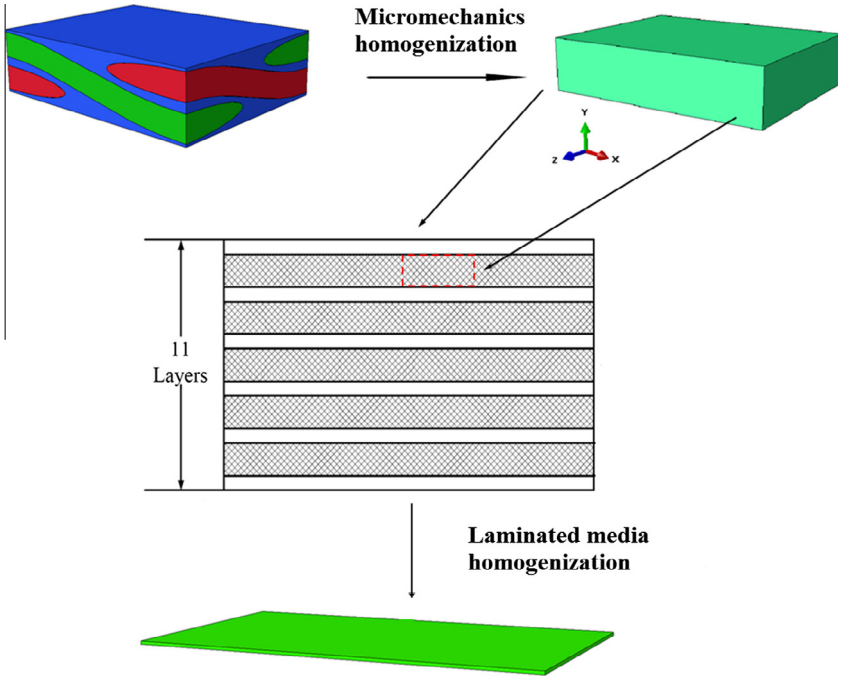

Fig. 11. Multilayer laminates homogenization process.

Table 5
Comparison of experimental and predicted multilayer PCB elastic modulus.

	E_{warp} (GPa)	Error (%) $\frac{E_{warp}-E_{experiment}}{E_{warp}}$	E_{fill} (GPa)	Error (%) $\frac{E_{fill}-E_{experiment}}{E_{fill}}$
Self-consistent scheme	33.6	3.3%	32.6	15.6%
Mori–Tanaka scheme	30.6.	−6.2%	29.1	3.2%
CCA/three phase scheme	31.1	−4.6%	29.6	4.9%
Experiment [22]	32.6	–	28.2	–

of the self-consistent scheme to accurately predict the property at high concentration of inclusions where interactions amongst inclusions are expected to be significant.

$$\begin{bmatrix}\varepsilon_1\\ \varepsilon_2\\ \varepsilon_3\\ \varepsilon_4\\ \varepsilon_5\\ \varepsilon_6\end{bmatrix} = \begin{bmatrix} \frac{1}{E_1} & -\frac{v_{21}}{E_2} & -\frac{v_{31}}{E_3} & & & \\ -\frac{v_{12}}{E_1} & \frac{1}{E_2} & -\frac{v_{32}}{E_3} & 0 & & \\ -\frac{v_{13}}{E_1} & -\frac{v_{23}}{E_2} & \frac{1}{E_3} & & & \\ & & & \frac{1}{G_{12}} & & \\ & 0 & & & \frac{1}{G_{13}} & \\ & & & & & \frac{1}{G_{23}} \end{bmatrix} \begin{bmatrix}\sigma_1\\ \sigma_2\\ \sigma_3\\ \sigma_4\\ \sigma_5\\ \sigma_6\end{bmatrix} \tag{8}$$

4. Multilayer PCB laminates homogenization

The effective property of a 1 mm thick multilayer circuit board (Fig. 10) containing six copper and five composite layers is considered in this section. The copper foil is of electrodeposited style and the associated pre-preg composite was of 7628 fabric style which was investigated in the previous sections.

Based on the effective properties of the composite ply from micromechanical homogenization, the multilayer PCB properties can be predicted through classical laminate theory (Appendix C). The procedure is illustrated in Fig. 11.

Table 5 compares our homogenized results with the experimental data from Low and Wang (2008), who conducted the mechanical test for the six-layer 7628 printed circuit board. Among the three schemes examined, the self-consistent scheme results in greater overestimation of Young's moduli, especially along the fill direction. Both Mori–Tanaka and CCA/three phase schemes yield better predictions compared to the experimental findings (Low and Wang, 2008). The difference could be attributed to geometrical approximations associated with FE modeling and possible rounding off errors. The results reveal that our current FE model based on Mori–Tanaka and CCA/three phase schemes is capable of predicting the elastic properties of multilayer printed circuit board.

5. Conclusions

In this paper, a novel hybrid micromechanics and FE modeling approach was used to determine the homogenized material property of a multilayer circuit board with wavy fiber bundles. A quarter of the periodic cell was selected as the FE model by applying symmetric, anti-symmetric and periodic boundary conditions at appropriate facets. The FE based unit cell boundary value problem was solved and the element based strain concentration matrices were computed. Various micromechanics schemes were used, examined and compared for the calculation of the equivalent properties of the composite substrate. Classical laminate theory was further adopted to obtain the homogenized properties of a multilayer printed circuit board. It was found that the self-consistent scheme results provide overestimation for the effective Young's modulus along the warp and fill directions. CCA/three phase and Mori–Tanaka schemes yielded better predictions which are in good agreement with existing experimental results. The newly proposed homogenization model can be used as an effective tool for the prediction of woven composite materials for multilayer PCB applications.

Acknowledgement

The authors would like to express their acknowledgment and appreciation to a private sponsor for funding the work and to Professor Marek-Jerzy Pindera from University of Virginia, USA, for his helpful suggestions.

Appendix A. Micromechanical relations

A.1. Self-consistent scheme

Plain strain bulk modulus:

$$k = k_m + c_f(k_f - k_m)\frac{k+\mu_T}{k_f+\mu_T} \tag{A.1}$$

Transverse shear modulus:

$$\frac{1}{\mu_T} = \frac{1}{\mu_m} + c_f\left(\frac{1}{\mu_f} - \frac{1}{\mu_m}\right)\frac{1+\frac{1-b}{b}}{1+\frac{\mu_T}{\mu_f}\left(\frac{1-b}{b}\right)} \tag{A.2}$$

$$b = \frac{k+2\mu_T}{2(k+\mu_T)} \tag{A.3}$$

Axial shear modulus:

$$\frac{1}{\mu_A} = \frac{1}{\mu_m} + c_f\left(\frac{1}{\mu_f} - \frac{1}{\mu_m}\right)\frac{2\mu_f}{(\mu_A+\mu_f)} \tag{A.4}$$

A.2. CCA model

Plain strain bulk modulus:

$$k = K_m + \frac{\mu_m}{3} + \frac{c_f}{3/\left(3K_f+\mu_f-3K_m-\mu_m\right)+3c_f/(3K_m+4\mu_m)} \tag{A.5}$$

Axial shear modulus:

$$\mu_A = \frac{\left(c_f\mu_f + c_m\mu_m + \mu_f\right)\mu_m}{c_m\mu_f + c_f\mu_m + \mu_m} \tag{A.6}$$

Axial Young's modulus:

$$E_A = c_fE_f + c_mE_m + \frac{4c_fc_m(v_f-v_m)^2\mu_m}{1+3c_f\mu_m/(3K_m+\mu_m)+3c_m\mu_m/(3K_f+\mu_f)} \tag{A.7}$$

Axial Poisson's ratio:

$$v_A = c_fv_f + c_mv_m + \frac{3c_fc_m(v_f-v_m)\mu_m\left[c_f\mu_m/(3K_m+\mu_m)+c_m\mu_m/(3K_f+\mu_f)\right]}{1+3c_f\mu_m/(3K_m+\mu_m)+3c_m\mu_m/(3K_f+\mu_f)} \tag{A.8}$$

A.3. Three phase model

Transverse shear modulus:

$$A\left(\frac{\mu_T}{\mu_m}\right)^2 + 2B\left(\frac{\mu_T}{\mu_m}\right) + C = 0 \tag{A.9}$$

$$\begin{aligned} A = {} & 3c(1-c)^2\left(\frac{\mu_f}{\mu_m}-1\right)\left(\frac{\mu_f}{\mu_m}+\eta_f\right) \\ & + \left[\frac{\mu_f}{\mu_m}\eta_m + \eta_f\eta_m - \left(\frac{\mu_f}{\mu_m}\eta_m - \eta_f\right)c^3\right] \\ & \times \left[c\eta_m\left(\frac{\mu_f}{\mu_m}-1\right) - \left(\frac{\mu_f}{\mu_m}\eta_m + 1\right)\right] \end{aligned} \tag{A.10}$$

$$\begin{aligned} B = {} & -3c(1-c)^2\left(\frac{\mu_f}{\mu_m}-1\right)\left(\frac{\mu_f}{\mu_m}+\eta_f\right) \\ & + \frac{1}{2}\left[\frac{\mu_f}{\mu_m}\eta_m + 1 + \left(\frac{\mu_f}{\mu_m}-1\right)c\right] \\ & \times \left[(\eta_m-1)\left(\frac{\mu_f}{\mu_m}+\eta_f\right) - 2\left(\frac{\mu_f}{\mu_m}\eta_m - \eta_f\right)c^3\right] \\ & + \frac{c}{2}(\eta_m-1)\left(\frac{\mu_f}{\mu_m}-1\right)\left[\frac{\mu_f}{\mu_m}\eta_m + \eta_f + \left(\frac{\mu_f}{\mu_m}-1\right)c^3\right] \end{aligned} \tag{A.11}$$

$$\begin{aligned} C = {} & 3c(1-c)^2\left(\frac{\mu_f}{\mu_m}-1\right)\left(\frac{\mu_f}{\mu_m}+\eta_f\right) \\ & + \left[\frac{\mu_f}{\mu_m} + \eta_f - \left(\frac{\mu_f}{\mu_m}\eta_m - \eta_f\right)c^3\right] \\ & \times \left[\frac{\mu_f}{\mu_m}\eta_m + 1 + \left(\frac{\mu_f}{\mu_m}-1\right)c\right] \end{aligned} \tag{A.12}$$

$$c = \left(\frac{a}{b}\right)^3, \quad \eta_m = 3 - 4\upsilon_m, \quad \eta_f = 3 - 4\upsilon_f \tag{A.13}$$

A.4. Mori–Tanaka model

Plain strain bulk modulus:

$$k = k_m + c_f(k_f - k_m)\frac{(k_m+\mu_m)}{(k_f+\mu_m)}\frac{1}{c_f\frac{(k_m+\mu_m)}{(k_f+\mu_m)} + (1-c_f)} \tag{A.14}$$

Transverse shear modulus:

$$\begin{aligned} \frac{1}{\mu_T} &= \frac{1}{\mu_m} + c_f\left(\frac{1}{\mu_f} - \frac{1}{\mu_m}\right)\frac{\bar{B}}{(c_f\bar{B} + (1-c_f))} \\ \bar{B} &= \frac{\bar{b}}{1 + \frac{\mu_m}{\mu_f}(\bar{b}-1)} \\ \bar{b} &= \frac{2(k_m+\mu_m)}{k_m + 2\mu_m} \end{aligned} \tag{A.15}$$

Axial shear modulus:

$$\frac{1}{\mu_A} = \frac{1}{\mu_m} + c_f\left(\frac{1}{\mu_f} - \frac{1}{\mu_m}\right)\frac{2\mu_f}{\mu_m+\mu_f}\frac{1}{\left(c_f\frac{2\mu_f}{\mu_m+\mu_f} + (1-c_f)\right)} \tag{A.16}$$

A.5. Hill's relations

$$E_A = c_m E_m + c_f E_f + \frac{4(\upsilon_m - \upsilon_f)^2}{\left(\frac{1}{k_m} + \frac{1}{k_f}\right)^2}\left[\left(\frac{c_f}{k_f} + \frac{c_m}{k_f}\right) - \frac{1}{k}\right] \tag{A.17}$$

$$\upsilon_A = c_m\upsilon_m + c_f\upsilon_f + \frac{(\upsilon_m - \upsilon_f)}{\left(\frac{1}{k_m} + \frac{1}{k_f}\right)}\left[\frac{1}{k} - \left(\frac{c_f}{k_f} + \frac{c_m}{k_f}\right)\right] \tag{A.18}$$

Appendix B. Periodic boundary condition implementation

B.1. Periodic boundary conditions

B.1.1. Normal strain loading

For the three sets of boundary conditions, the displacements imposed on the symmetric boundaries of FE unit cell are:

$$\begin{aligned} & S_4 : u_1(X, y_1, z_1) = 0 \\ & S_6 : u_3(x_1, y_1, Z) = 0 \end{aligned} \tag{B.1}$$

1. Apply $\bar{\varepsilon}_{11} \neq 0$, all others zero:

$$\begin{aligned} & S_1 : u_1(X, y_1, z_1) = \bar{\varepsilon}_{11}X \\ & S_3 : u_3(x_1, y_1, Z) = 0 \\ & S_2 \ \& \ S_5 : u_2(x_1, Y, z_1) - u_2(x_1, 0, z_1) = 0 \end{aligned} \tag{B.2}$$

2. Apply $\bar{\varepsilon}_{22} \neq 0$, all others zero:

$$\begin{aligned} & S_1 : u_1(X, y_1, z_1) = 0 \\ & S_3 : u_3(x_1, y_1, Z) = 0, \\ & S_2 \ \& \ S_5 : u_2(x_1, Y, z_1) - u_2(x_1, 0, z_1) = \bar{\varepsilon}_{22}Y \end{aligned} \tag{B.3}$$

3. Apply $\bar{\varepsilon}_{33} \neq 0$, all others zero:

$$\begin{aligned} & S_1 : u_1(X, y_1, z_1) = 0 \\ & S_3 : u_3(x_1, y_1, Z) = \bar{\varepsilon}_{33}Z \\ & S_2 \ \& \ S_5 : u_2(x_1, Y, z_1) - u_2(x_1, 0, z_1) = 0 \end{aligned} \tag{B.4}$$

B.1.2. Shear strain loading

For the three sets of boundary conditions, the displacements imposed on the anti-symmetric boundaries of FE unit cell are:

$$\begin{aligned} & S_4 : u_2(X, y_1, z_1) = 0, \quad u_3(X, y_1, z_1) = 0 \\ & S_6 : u_1(x_1, y_1, Z) = 0, \quad u_2(x_1, y_1, Z) = 0 \end{aligned} \tag{B.5}$$

4. Apply $\bar{\varepsilon}_{23} \neq 0$, all others zero:

$$\begin{aligned} & S_1 : u_1(X, y_1, z_1) = 0 \\ & S_3 : u_2(x_1, y_1, Z) = \bar{\varepsilon}_{32}Z \\ & S_2 \ \& \ S_5 : u_2(x_1, Y, z_1) - u_2(x_1, 0, z_1) = 0 \\ & u_3(x_1, Y, z_1) - u_3(x_1, 0, z_1) = \bar{\varepsilon}_{23}Y \end{aligned} \tag{B.6}$$

5. Apply $\bar{\varepsilon}_{13} \neq 0$, all others zero:

$$\begin{aligned} & S_1 : u_3(X, y_1, z_1) = \bar{\varepsilon}_{13}X \\ & S_3 : u_1(x_1, y_1, Z) = \bar{\varepsilon}_{31}Z \\ & S_2 \ \& \ S_5 : u_2(x_1, Y, z_1) - u_2(x_1, 0, z_1) = 0 \end{aligned} \tag{B.7}$$

6. Apply $\bar{\varepsilon}_{12} \neq 0$, all others zero:

$$\begin{aligned} & S_1 : u_2(X, y_1, z_1) = \bar{\varepsilon}_{12}X \\ & S_3 : u_3(x_1, y_1, Z) = 0 \\ & S_2 \ \& \ S_5 : u_2(x_1, Y, z_1) - u_2(x_1, 0, z_1) = 0 \\ & u_1(x_1, Y, z_1) - u_1(x_1, 0, z_1) = \bar{\varepsilon}_{21}Y \end{aligned} \tag{B.8}$$

Appendix C. Classical laminate theory

The homogenized equivalent elastic constants can be written in terms of constants of each individual layer. The equivalent elastic constants are obtained as:

$$C_{ij} = \sum_{k=1}^{n}\upsilon^k\left(C_{ij}^k - \frac{C_{i3}^k C_{3j}^k}{C_{33}^k} + \frac{C_{i3}^k\sum_{l=1}^{n}\frac{\upsilon^l C_{3j}^l}{C_{33}^l}}{C_{33}^k\sum_{l=1}^{n}\frac{\upsilon^l}{C_{33}^l}}\right) \tag{C.1}$$

$$C_{ij} = C_{ji} = 0, \quad i = 1,2,3,6;\ j = 4,5 \tag{C.2}$$

$$C_{ij} = \frac{\sum_{k=1}^{n} \frac{v^k}{\Delta'_k} C_{ij}}{\sum_{k=1}^{n}\sum_{l=1}^{n} \frac{v^k v^l}{\Delta'_k \Delta'_l}\left(C^k_{44}C^l_{55} - C^k_{45}C^l_{54}\right)}, \quad i,j = 4,5 \tag{C.3}$$

$$\text{where, } \Delta'_k = \begin{vmatrix} C^k_{44} & C^k_{45} \\ C^k_{54} & C^k_{55} \end{vmatrix} \tag{C.4}$$

$$v^k = \frac{\text{volume of material } k}{\text{volume of composite element}} \tag{C.5}$$

References

Blackketter, D.M., Walrath, D.E., Hansen, A.C., 1993. Modeling damage in a plain weave fabric-reinforced composite material. J. Compos. Technol. Res. 15 (2), 136–142.

Christensen, R.M., Lo, K.H., 1979. Solutions for effective shear properties in three phase sphere and cylinder models. J. Mech. Phys. Solids 27 (4), 315–330.

Cowin, S.C., 2013. Continuum Mechanics of Anisotropic Materials. Springer.

Dasgupta, A., Agarwal, R.K., Bhandarkar, S.M., 1996. Three-dimensional modeling of woven-fabric composites for effective thermo-mechanical and thermal properties. Compos. Sci. Technol. 56 (3), 209–223.

Harris, C.M., Pierosol, A.G., 2002. Harris's Shock and Vibration Handbook. McGraw-Hill, New York.

Hashin, Z., 1965. On elastic behaviour of fibre reinforced materials of arbitrary transverse phase geometry. J. Mech. Phys. Solids 13 (3), 119–134.

Hil, R., 1965. Theory of mechanical properties of fibre-strengthened materials—III. Self-consistent model. J. Mech. Phys. Solids 13 (4), 189–198.

Ishikawa, T., Chou, T.W., 1982a. Stiffness and strength behaviour of woven fabric composites. J. Mater. Sci. 17 (11), 3211–3220.

Ishikawa, T., Chou, T.W., 1982b. Elastic behavior of woven hybrid composites. J. Compos. Mater. 16, 2–19.

Ishikawa, T., Chou, T.W., 1983a. One-dimensional micromechanical analysis of woven fabric composites. AIAA J. 21 (12), 1714–1721.

Ishikawa, T., Chou, T.W., 1983b. In-plane thermal expansion and thermal bending coefficients of fabric composites. J. Compos. Mater. 17 (2), 92–104.

Ito, M., Chou, T.W., 1997. Elastic moduli and stress field of plain-weave composites under tensile loading. Compos. Sci. Technol. 57 (7), 787–800.

Lee, M., 2000. Finite element modeling of printed circuit boards (PCBs) for structural analysis. Circuit World 26 (3), 24–29.

Lee, J.W., Harris, C.E., 1988. A micromechanics model for the effective Young's modulus of a piecewise-isotropic laminate with wavy patterns. J. Compos. Mater. 22 (8), 717–741.

Low, K.H., Wang, Y., 2008. Hybrid modeling of woven fibre reinforced metal matrix composite for multilayer circuit boards. Circuit World 34 (2), 12–20.

Mori, T., Tanaka, K., 1973. Average stress in matrix and average elastic energy of materials with misfitting inclusions. Acta Metall. 21 (5), 571–574.

Naik, N.K., Shembekar, P.S., 1992a. Elastic behavior of woven fabric composites: I—lamina analysis. J. Compos. Mater. 26 (15), 2196–2225.

Naik, N.K., Shembekar, P.S., 1992b. Elastic behavior of woven fabric composites. III. Laminate design. J. Compos. Mater. 26 (17), 2522–2541.

Naik, N.K., Shembekar, P.S., 1993. Elastic analysis of woven fabric laminates. II. Mixed fabric laminates. J. Compos. Technol. Res. 15 (1), 34–37.

Sankar, B.V., Marrey, R.V., 1993. A unit-cell model of textile composite beams for predicting stiffness properties. Compos. Sci. Technol. 49 (1), 61–69.

Shindo, Y., Ueda, S., Nishioka, Y., 1993. Mechanical behavior of woven composites at low temperatures. Fusion Eng. Des. 20, 469–474.

Shrotriya, P., 2001. Dimensional stability of multilayer circuit boards (PhD thesis). University of Illinois at Urbana-Champaign.

Sottos, N.R., Ockers, J.M., Swindeman, M., 1999. Thermoelastic properties of plain weave composites for multilayer circuit board applications. J. Electron. Packag. 121 (1), 37–43.

Wang, Y.Q., Low, K.H., Che, F.X., Pang, H.L.J., Yeo, S.P., 2003. Modeling and simulation of printed circuit board drop test. Electron. Packag. Technol. Conf., 263–268.

Wang, Y., Low, K.H., Pang, H.L.J., Hoon, K.H., Che, F.X., Yong, Y.S., 2006. Modeling and simulation for a drop-impact analysis of multi-layered printed circuit boards. Microelectron. Reliab. 46 (2), 558–573.

Zhu, Q., Shrotriya, P., Sottos, N.R., Geubelle, P.H., 2003. Three-dimensional viscoelastic simulation of woven composite substrates for multilayer circuit boards. Compos. Sci. Technol. 63 (13), 1971–1983.